

# Nanoscale

Accepted Manuscript



This is an *Accepted Manuscript*, which has been through the Royal Society of Chemistry peer review process and has been accepted for publication.

*Accepted Manuscripts* are published online shortly after acceptance, before technical editing, formatting and proof reading. Using this free service, authors can make their results available to the community, in citable form, before we publish the edited article. We will replace this *Accepted Manuscript* with the edited and formatted *Advance Article* as soon as it is available.

You can find more information about *Accepted Manuscripts* in the [Information for Authors](#).

Please note that technical editing may introduce minor changes to the text and/or graphics, which may alter content. The journal's standard [Terms & Conditions](#) and the [Ethical guidelines](#) still apply. In no event shall the Royal Society of Chemistry be held responsible for any errors or omissions in this *Accepted Manuscript* or any consequences arising from the use of any information it contains.

# Donor-Acceptor Cocrystal Based on Hexakis(alkoxy)triphenylene and Perylenediimide Derivatives with Ambipolar Transporting Property

Yajun Su, Yan Li, Jiangang Liu, Rubo Xing and Yanchun Han\*

State Key Laboratory of Polymer Physics and Chemistry, Changchun Institute of Applied Chemistry, Chinese Academy of Sciences, 5625 Renmin Street, Changchun 130022, P. R. China;

University of the Chinese Academy of Sciences, No.19A Yuquan Road, Beijing 100049, China.

Tel: 86-431-85262175, Fax: 86-431-85262126, Email: [ychan@ciac.ac.cn](mailto:ychan@ciac.ac.cn)

\* To whom correspondence should be addressed

**ABSTRACT:** Organic donor-acceptor cocrystal with ambipolar transporting property was constructed based on N,N'-bis(1-ethylpropyl)-perylene-3,4,9,10-tetracarboxylic diimide (EP-PDI) and 2,3,6,7,10,11-hexakis-(hexyloxy)-triphenylene (H6TP). Cocrystal with alternating stacking of H6TP and EP-PDI molecules was formed through both drop-casting and spin-coating processes, especially at optimized ratio of H6TP/EP-PDI (2/1, 1/1). The formation of the cocrystal was driven by the strong  $\pi$ - $\pi$  interaction and the weaker steric hindrance, resulting from the smaller side groups, between the donor and acceptor molecules. Field effect transistors (FETs) based on

H6TP/EP-PDI cocrystal exhibited relatively balanced hole/electron transport, with hole mobility of  $1.14 \times 10^{-3} \text{ cm}^2 \text{ V}^{-1} \text{ s}^{-1}$  and electron mobility of  $1.40 \times 10^{-3} \text{ cm}^2 \text{ V}^{-1} \text{ s}^{-1}$ .

**KEYWORDS:** organic cocrystal, 2,3,6,7,10,11-hexakis-(hexyloxy)-triphenylene (H6TP), N,N'-bis(1-ethylpropyl)-perylene-3,4,9,10-tetracarboxylic diimide (EP-PDI), donor-acceptor mixture,  $\pi$ - $\pi$  interaction, ambipolar transport

## 1. Introduction

Over several decades, much interest has been focused on organic donor and acceptor blends. Supramolecular structure based on the mixing of p- and n- type semiconductors has been shown benefit for the improvement of the performances of organic photovoltaics.<sup>1-2</sup> Besides, donor-acceptor cocrystals could also potentially applied in other fields, due to their special structures. Organic cocrystals with alternating stacking of donor and acceptor have been demonstrated suitable for ambipolar transport of charge in the field of organic field effect transistor (OFET), both in theory and experiment.<sup>3-6</sup> Room temperature ferroelectricity has also been reported in mixed-stacked donor-acceptor cocrystal.<sup>7</sup> Although various donor-acceptor pairs for the formation of cocrystals have been reported, the investigation of the formation mechanism remain challenging. In order to construct organic donor-acceptor cocrystals, a strong interaction between the donor and acceptor molecules should exist to suppress the crystallization of individual component. Besides, structural complementation or similarity may be also essential.

According to the literatures, the driving forces for the assembly of organic cocrystal were hydrogen bond<sup>8-10</sup>,  $\pi$ - $\pi$  interaction<sup>11-12</sup> and charge transfer between the donor and acceptor<sup>13-14</sup>. As common n- type semiconductors possessing typical spherical structures, C<sub>60</sub>/C<sub>70</sub> and PCBM ([6,6]-phenyl-C70-butyricacidmethylester) have been used to assemble with substituted contorted hexabenzocoronene (12-c-HBC)<sup>2</sup>, sulfur-bridged annulene<sup>6</sup> and porphyrin derivatives<sup>15-16</sup>. All the donor molecules have hollow structures which are complementary with spherical C<sub>60</sub>/C<sub>70</sub> and PCBM, making the supramolecular assembly available. Besides, donor/acceptor pair with similar symmetry and structure also showed remarkable assembled property, resulting in typical organic cocrystal.<sup>5, 17</sup> Being the hotspot of the investigation, discotic donor and acceptor molecules have shown superior interaction between the components. In the solution, strong charge transfer (CT) state often formed, accompany with obvious color change.<sup>13-14</sup> The CT interaction in the solution induced significant morphological difference of the complex, compared to the individual component. Other than CT state, stable extended stacks of discotic donor and acceptor molecules have been reported, due to the charge complementation between the  $\pi$ -rich and  $\pi$ -poor aromatic systems, especially when the mixing components have similar structural symmetry.<sup>18-19</sup> However, because most of the discotic molecules possess liquid crystalline property, the present work mainly focuses on the extension of mesophase temperature, through mixing of discotic p- and n- type molecules.<sup>20</sup> Less attention has been paid on the crystalline structure of donor-acceptor complexes. Another impressive point was that the electronic transport property could be improved in

complementary discotic binary mixture, due to the formation of ordered supramolecular structure.<sup>21-24</sup> Although the search of suitable donor/acceptor pairs for the fabrication of organic cocrystals remain difficult, discotic  $\pi$ -rich and  $\pi$ -poor molecules with large conjugated plane seem to be desired candidates.<sup>25-26</sup> The large electrical complementation and  $\pi$ - $\pi$  interaction between the donor/acceptor pair may be the driving force.

Taking the conclusion into account, two discotic molecules, N,N'-bis(1-ethylpropyl)-perylene-3,4,9,10-tetracarboxylic diimide (EP-PDI) and 2,3,6,7,10,11-hexakis-(hexyloxy)-triphenylene (H6TP), were chosen, in order to investigate the assembly character of the donor/acceptor pair. We focused on the crystalline structure of the blended film and found that cocrystal with alternating stacking of H6TP and EP-PDI molecules was formed. Based on the characterizations of the solution and film, we argued that the strong  $\pi$ - $\pi$  interaction and weaker steric hindrance between H6TP and EP-PDI molecules were responsible for the formation of the cocrystal. Relatively balanced hole/electron transport was also observed in FETs based on H6TP/EP-PDI cocrystal.

## 2. Experimental Section

### 2.1 Materials:

H6TP was purchased from Keqing Zhao group, Sichuan Normal University. EP-PDI was supplied by Yanhou Geng group, Changchun Institute of Applied Chemistry. The chemical structures of H6TP and EP-PDI are shown in Scheme 1. The

materials could be synthesized following the routes reported in Reference 27 and 28. Chlorobenzene (CB, 99%) and chloroform (99%) were purchased from Beijing Chemical, China. The physical parameters of the solvents were summed in Table 1. All the materials were used as received without further purification.

The glass substrates were cleaned in a piranha solution (70/30 v/v of concentrated  $\text{H}_2\text{SO}_4$  and 30%  $\text{H}_2\text{O}_2$ ) at  $90^\circ\text{C}$  for 20 min, then thoroughly rinsed with deionized water, and finally blown dry under nitrogen. Highly doped n-type Si wafers with a 300 nm thermally grown oxide layer were rinsed in deionized water, ethanol and acetone, successively, and blown dry under nitrogen.

## 2.2 Sample Preparation:

H6TP and EP-PDI were dissolved in chloroform and chlorobenzene with concentrations of 5 mg/ml, respectively. H6TP/EP-PDI solutions with different ratios by weight were prepared by mixing the individual solutions. Before used all the solutions were placed at room temperature overnight for the complete dissolution of the solutes.

Spin-coating and drop-casting were used to prepare H6TP, EP-PDI and the blended films. In the spin-coating procedure, the solution was cast for 60 s at a rate of 1250 rpm. In the drop-casting process, 50  $\mu\text{l}$  solution was deposited on the glass substrate with a size of 1.5 cm $\times$ 1.5 cm. All the experiments were performed at room temperature. The obtained film thicknesses in spin-coating and drop-casting procedures were 75-90 nm and 850-900 nm, respectively.

## 2.3 Characterization:

The solution state of H6TP, EP-PDI and EP-PDI blend were characterized through UV-vis absorption spectroscopy, fluorescence emission spectra and nuclear magnetic resonance ( $^1\text{H}$  NMR). Polarized optical microscopy (POM), fluorescence optical microscopy, atomic force microscopy (AFM), transmission electron microscopy (TEM), selected area electron diffraction (SAED), grazing incidence X-ray diffraction (GIXD), in-plane XRD, fluorescence spectra and UV-vis absorption spectroscopy were performed to characterize the morphologies and structures of the corresponding crystalline films. Differential scanning calorimetry (DSC) was performed to characterize the thermal properties of H6TP, EP-PDI and H6TP/EP-PDI blend.

$^1\text{H}$  NMR spectra were recorded on Bruker AV 300 spectrometer in  $\text{CDCl}_3$  with tetramethylsilane (TMS) as the internal reference.

The fluorescence emission spectra of the solutions and films were obtained using a Perkin-Elmer LS 55 luminescence spectrometer.

UV-vis absorption spectroscopy was recorded with a Lambda 750 spectrometer (Perkin-Elmer, Wellesley, MA).

Both the POM and fluorescence microscopy images were taken with a polarized optical microscopy (Zeiss Axio Imager A2m, Carl Zeiss, Germany). POM images were obtained in reflection mode through two crossed polarizers. Fluorescence microscopy images were obtained when mercury lamp with excitation wavelength of 365 nm was used as the light source.

AFM images were obtained using a SPA-300HV instrument with a SPI3800N Controller (Seiko Instruments Inc., Japan) in tapping mode. A silicon microcantilever

(spring constant 2 N/m and resonant frequency  $\approx 70$  kHz, Olympus, Japan) was used for the scanning.

TEM images and SAED patterns were obtained with a JEOL JEM-1011 transmission electron microscope operated at an accelerating voltage of 100 kV. For TEM characterization, the films were floated from the glass substrates with deionized water and picked up with copper grids.

GIXD pattern was obtained on Bruker D8 Discover Reflector (Cu  $K\alpha$ ,  $\lambda=1.54056$  Å) under 40 kV and 40 mA tube current. The X-ray profile was recorded from 2 to 20 degree with a step of 0.05 degree using automatic slits.

In-plane XRD pattern was obtained on SmartLab X-ray diffractometer (Rigaku, Cu  $K\alpha$ ,  $\lambda=1.54056$  Å). The X-ray profile was recorded from 2 to 30 degree with a step of 0.05 degree using automatic slits.

DSC was performed on a TA DSC Q2000. Both the heating and cooling rates were set to 10°C/min.

#### **2.4 OFET Device Fabrication:**

To fabricate OFET devices, highly doped n-type Si wafers with a 300 nm thermally grown oxide layer were used as the substrates. To prepare the semiconductor layer, both spin-coating and drop-casting methods were used. The ratio of H6TP/EP-PDI was set to be 1/1. The concentration of H6TP/EP-PDI solution in chloroform was 5 mg/ml. The gold source-drain electrodes were deposited by thermal evaporation in high vacuum ( $\sim 8 \times 10^{-4}$  Pa) to finish the preparation of OFETs.

I-V curves were measured to characterize the performances of OTFTs. Field-effect

characteristic measurements were carried out on a Keithley 4200 semiconductor parameter analyzer under ambient conditions.

### **3. Results and Discussion**

In the following part, we depict the fabrication of organic donor-acceptor cocrystal based on H6TP and EP-PDI molecules. The morphology and crystalline structure of the cocrystal will be described. The mechanism for the formation of the cocrystal is also expounded in detail through the characterizations of the solution state and film structure. Ambipolar transport property of the cocrystal is observed based on the preparation of OFET device.

#### **3.1 The Fabrication of Donor-Acceptor Cocrystal Based on H6TP and EP-PDI molecules**

##### **3.1.1 The Morphology of H6TP/EP-PDI Film**

The films of H6TP, EP-PDI and H6TP/EP-PDI blends with different ratios by weight were firstly prepared through drop-casting method, in which chloroform was used as the solvent. The morphologies of the crystalline films were shown in Figure 1. As it can be seen, H6TP molecules assembled into long ribbon-like crystals. In EP-PDI film, short rod-like crystals could be observed, which were similar to the crystalline morphology of other perylenediimide derivative.<sup>29</sup> However, in H6TP/EP-PDI films, the crystalline morphologies changed dramatically. Sheet crystals were obtained, which dominated in the films. The morphology was somewhat like that of spherulite, as can be seen in Figure 1e. The individual crystals of H6TP

and EP-PDI with specific shapes could hardly be seen. The significant morphological difference between the blended and the individual films of H6TP and EP-PDI indicated that the crystallization of the individual component was suppressed by the other constituent. A new type of crystal may be formed in this situation. We argued that H6TP and EP-PDI molecules assembled together with certain ratio, and that was why the crystalline morphologies of the blends were different from that of the individual component. Typically, as the ratios of H6TP/EP-PDI were 1/2, 1/3 and 1/4, where the content of EP-PDI may be excessive for the assembly, we observed the coexistence of EP-PDI crystals with the sheet crystals. The crystals of EP-PDI were marked in the white boxes of Figure S1.

Spin-coating process was used to investigate the microstructure of H6TP, EP-PDI and the blended films. When chloroform was used as the solvent, crystalline films were all obtained. As it can be seen in Figure S2, the domain sizes of the crystals were small, due to the fast evaporation of the solvent in the procedure of spin-coating. The corresponding AFM images of the films were shown in Figure 2a. In EP-PDI film, grainy crystallites with sizes of hundreds of nanometers were observed. While elongated crystallites were obtained in H6TP film. In the blended films with ratios of 2/1 and 1/1, the morphologies were somewhat different, and the domain sizes became a little smaller. TEM images were also shown, from which we could see the morphological difference between H6TP/EP-PDI (2/1, 1/1) films and the film of the individual component. The corresponding SAED patterns of these films were also different. In H6TP film, diffraction matrix was observed, indicating the good

crystallinity of the film. It was worth to mention that many high-order diffractive points appeared in the pattern, resulting from the high order in the crystal. For EP-PDI film, two diffractive rings were obtained. The inter-planar distances corresponding to the inner and outer rings were calculated to be 0.37 nm and 0.35 nm, respectively. However, in the blended film, the diffractive points of H6TP disappeared, replaced by a single diffractive ring, corresponding to an inter-planar distance of 0.38 nm. It could be attributed to the diffraction of  $\pi$ - $\pi$  stacking plane. We could thus conclude that in H6TP/EP-PDI film, the crystallization of H6TP was suppressed, and organic cocrystal may form.

Chlorobenzene was also used as the solvent to study the influence on the morphology of H6TP/EP-PDI film. The POM images of the drop-cast films were shown in Figure S3. Short needle-like and long ribbon-like crystals were obtained in EP-PDI and H6TP film, respectively. In the blended films, sheet crystals were observed, which were different from that of EP-PDI and H6TP crystals. Besides, as also shown in Figure S3, when excited using mercury lamp with wavelength of 365 nm, red and blue fluorescence patterns were observed in EP-PDI and H6TP films, respectively. However, no fluorescence pattern was obtained in the blended film. The fluorescence quenching indicated that a strong charge-transfer interaction must exist in the film, which may be result from the formation of H6TP/EP-PDI cocrystal. In the spin-coating procedure, as can be seen in Figure S5, small crystallites formed in EP-PDI film. In H6TP film, discrete ribbon-like crystals were observed, due to the poor film-forming property of the molecule when chlorobenzene was used as the

solvent. Fan-like crystals were obtained in the blended film. The typical shape of the crystal may indicate the formation of H6TP/EP-PDI cocrystal.

### 3.1.2 The Crystalline Structure of H6TP/EP-PDI Film

XRD was performed to investigate the crystalline structures of H6TP/EP-PDI films. When chloroform was used as the solvent, the GIXD profiles of drop-cast films were shown in Figure 3a1. In EP-PDI film, a strong diffractive peak at  $2\theta=5.35^\circ$ , corresponding to an inter-planar distance of  $16.51 \text{ \AA}$ , was observed. We could attribute the peak to the (200) diffraction of EP-PDI crystal, as reported in the literature<sup>30</sup>. A wide weak diffractive peak at  $2\theta=10.70^\circ$ , corresponding to an inter-planar distance of  $8.26 \text{ \AA}$  could also be seen. It could be attributed to the (400) diffraction of EP-PDI crystal, which was the secondary of the (200) peak. We could thus conclude that in the crystalline film, EP-PDI molecules arranged mainly with *a* axis perpendicular to the substrate. It was also worth to mention that an additional weak diffractive peak at  $2\theta=8.11^\circ$ , corresponding to an inter-planar distance of  $10.91 \text{ \AA}$ , was present. It corresponded to the (002) diffraction of EP-PDI crystal, which indicated that some of the molecules oriented with *c* axis perpendicular to the substrate. The coexistence of both (200) and (002) diffraction demonstrated that EP-PDI molecules arranged with two types of orientation in the normal direction of the substrate. The phenomenon could be attributed to the fast evaporation of the solvent, due to the rather low boiling point ( $61.3^\circ\text{C}$ ) of chloroform. In H6TP film, a strong diffractive peak at  $2\theta=4.76^\circ$ , corresponding to an inter-planar distance of  $18.54 \text{ \AA}$  was observed. It could be attributed to the (001) diffraction of H6TP crystal<sup>31</sup>.

An additional weak diffractive peak at  $2\theta=6.34^\circ$ , corresponding to an inter-planar distance of  $13.92 \text{ \AA}$ , could also be obtained, which may be the (010) diffraction of H6TP crystal. Similar to the situation in EP-PDI film, the appearance of the weak additional peak was induced by the incomplete orientation of H6TP molecules in the perpendicular direction. However, when H6TP was blended with EP-PDI molecules, the diffraction of the film became different. The diffractive peak of the individual component nearly vanished, and a new strong diffractive peak appeared. As XRD was the most forceful means to characterize the formation of organic cocrystal<sup>17</sup>, we could thus argue that H6TP and EP-PDI molecules assembled together, and a cocrystal may be obtained. The conclusion could also be supported by the different morphology of the blend film, compared to the crystal of individual constituent, as aforementioned. Base on the different diffractive profiles at various ratios of H6TP/EP-PDI, we could see that the optimized ratios for the co-assembly were 2/1 and 1/1. At these ratios, nearly single diffractive peak was observed, which appeared at  $2\theta=5.99^\circ$ , corresponding to an inter-planar distance of  $14.75 \text{ \AA}$ , as it can be seen in Figure 3a2. The diffractive peak was very different from that of H6TP and EP-PDI crystals, indicating the cocrystal dominated in the blended film. When the content of H6TP was excessive (H6TP/EP-PDI=4/1, 3/1), a strong diffractive peak at  $2\theta=5.86^\circ$ , corresponding to an inter-planar distance of  $15.10 \text{ \AA}$ , was observed. Besides, a wide diffractive peak at  $2\theta=4.50-5.18^\circ$  was also visible. The diffractive profile may result from the overlapping of the diffractive peaks of H6TP/EP-PDI cocrystal and the redundant H6TP crystals. On the other hand, when the content of EP-PDI was

excessive (H6TP/EP-PDI=1/2, 1/3, 1/4), the diffractive peak at  $5.99^\circ$  became weaker, and the diffractive peak at  $5.40^\circ$  became stronger. It may be attributed to the coexistence of H6TP/EP-PDI cocrystal and individual EP-PDI crystals. The results were accordant to the POM images, from which we could see EP-PDI crystals at high EP-PDI ratios. Based on the discussion, we determined the optimized H6TP/EP-PDI ratios for the fabrication of the cocrystal were 2/1 and 1/1.

In-plane XRD was further performed to characterize the in-plane crystalline structure of H6TP/EP-PDI films, the result of which was shown in Figure 3b1. In H6TP film, two strong diffractive peaks at  $2\theta=4.30^\circ$  and  $2\theta=5.99^\circ$  were observed. The corresponding inter-planar distances were 20.52 Å and 14.75 Å, respectively. As H6TP molecules arranged mainly with *c* axis perpendicular to the substrate, according to the GIXD result, the peak at  $2\theta=5.99^\circ$  may be attributed to the (010) diffraction in the horizontal direction. While the peak at  $2\theta=4.30^\circ$  could be attributed to the (001) diffraction, due to the incomplete orientation of H6TP molecules. The weak peaks at  $2\theta=8.91^\circ$ ,  $11.80^\circ$  and  $18.01^\circ$  may be the higher-order diffractions of the (001) lattice plane. A diffractive peak at  $2\theta=20.96^\circ$ , corresponding to an inter-planar distance of 4.25 Å, was also observed. It was similar to the slipped  $\pi$ - $\pi$  stacking in H6TP crystal. In EP-PDI crystal, because the molecules oriented mainly with *a* axis perpendicular to the substrate, we obtained the (002) diffraction in the in-plane XRD profile, which appeared at  $2\theta=8.01^\circ$ , corresponding to an inter-planar distance of 16.65 Å. It was reasonable that an additional diffractive peak at  $2\theta=5.30^\circ$  was also observed. It could be attributed to

the (200) diffraction of EP-PDI crystal, considering that some of the molecules arranged with  $c$  axis in the perpendicular direction, based on the GIXD result. Other peaks may be the higher-order diffractions of the lattice planes. However, in the blended films, the diffractive profiles changed dramatically. A strong peak at  $2\theta=25.80^\circ$  was conspicuous, corresponding to an inter-planar distance of 3.45 Å. It could be attributed to the diffraction of  $\pi$ - $\pi$  stacking. The peak was extremely intense when the ratios of H6TP/EP-PDI were 2/1 and 1/1, as shown in Figure 3b2. We could also see that the diffractive peaks of H6TP and EP-PDI crystals were suppressed, indicating the formation of organic cocrystal. A new diffractive peak at  $2\theta=5.01^\circ$ , corresponding to an inter-planar distance of 17.11 Å, was observed. It was different from the diffraction based on the individual crystal of H6TP and EP-PDI. We could thus conclude that the cocrystal arranged with a different in-plane order. The optimized ratios of H6TP/EP-PDI for the co-assembly could also be determined to be 2/1 and 1/1, based on the in-plane XRD results. When a component, for example EP-PDI, was excessive, the diffractive peak of the individual crystal ( $2\theta=8.01^\circ$ ) could also be seen.

For the films spin-coated from corresponding chloroform solutions, the GIXD profiles were shown in Figure 2b. Diffractive peaks at  $2\theta=4.87^\circ$  and  $2\theta=8.09^\circ$  were observed for H6TP and EP-PDI films, respectively. It indicated that both H6TP and EP-PDI molecules arranged with  $c$  axis perpendicular to the substrate, as discussed earlier. In the blended film, the diffractive peak of the individual component vanished, and a single strong diffractive peak appeared at  $2\theta=5.90^\circ$ - $6.08^\circ$ . Similar

to the XRD profiles of the drop-cast films, it was a forceful evidence for the formation of H6TP/EP-PDI cocrystal. We demonstrated that H6TP and EP-PDI molecules co-assembled into donor-acceptor cocrystal in both drop-casting and spin-coating processes.

When chlorobenzene was used as the solvent, the situation was similar. In drop-cast blended films, from GIXD profiles, we could see the diffractive peaks of H6TP and EP-PDI crystals vanished, and a new peak of the cocrystal appeared, as shown in Figure S4. As also can be seen in Figure S4, we found that the diffractive peak of  $\pi$ - $\pi$  stacking plane ( $2\theta=25.8^\circ$ ) existed in the blended film, based on the in-plane XRD result. According to XRD profiles, we concluded that H6TP/EP-PDI cocrystal was formed. GIXD result of spin-coated films was shown in Figure S6, from which we observed a new diffractive peak in H6TP/EP-PDI film, different from that of the individual crystal. It was also an evidence for the formation of H6TP/EP-PDI cocrystal.

Based on the POM images, SAED patterns, GIXD and in-plane XRD profiles, we ensured that in the blended film, H6TP and EP-PDI molecules assembled into organic cocrystal. The crystallization of the individual component was inhibited. The optimized ratios of H6TP/EP-PDI were 2/1 and 1/1, which were mainly used in the work. Typically, the intense diffraction of  $\pi$ - $\pi$  stacking in the in-plane XRD profile indicated that strong  $\pi$ - $\pi$  interaction exist between H6TP and EP-PDI molecules, which may be the driving force for the formation of the complex. Besides, according to the discussion, we argued that the preparation of H6TP/EP-PDI cocrystal was not

influenced by the selection of the solvent, although the morphology may be somewhat different. The same crystalline structure could be formed, based on the similar diffraction of the films processed through chloroform and chlorobenzene.

We could depict the crystalline structures of EP-PDI, H6TP and H6TP/EP-PDI cocrystal, the schematic diagrams of which were shown in Figure 4. In EP-PDI film, the diffractive peaks in GIXD and in-plane XRD profiles were accordant to that reported in the literature<sup>30</sup>. Thus in the crystal, EP-PDI molecules mainly arranged with *a* axis perpendicular to the substrate. A “herringbone-like” structure was deduced, as shown in Figure 4a. Similarly, the arrangement of H6TP molecules could be depicted in Figure 4b, according to the reported lattice parameters<sup>31</sup>.

In H6TP/EP-PDI cocrystal, the crystallization of the single component was suppressed, based on the disappearance of the individual diffractive peaks. New diffractive peaks were observed in both GIXD and in-plane XRD profiles, which indicated that alternating stacking of H6TP and EP-PDI molecules was formed. The schematic structure was shown in Figure 4c. The donor and acceptor molecules stacked into crystalline columns through  $\pi$ - $\pi$  interaction, with an inter-planar distance of 3.4 Å. The in-plane and out-of-plane spacings between the columns were determined to be 17.11 Å and 14.75 Å, respectively, according to the obtained diffractive peaks at  $2\theta=5.01^\circ$  and  $2\theta=5.99^\circ$  in the in-plane XRD and GIXD profiles.

## 3.2 The Formation Mechanism of H6TP/EP-PDI Cocrystal

### 3.2.1 The Exclusion of Charge Transfer Interaction between H6TP and EP-PDI

### Molecules in Solution

In order to clarify the formation mechanism of H6TP/EP-PDI cocrystal, the solution state was firstly characterized. In our experiment, we did not observe obvious color change after blended H6TP into EP-PDI solution. The phenomenon was unlike that reported in the literatures<sup>13, 14, 17</sup>, where strong donor-acceptor charge transfer (CT) state formed in the solution. The UV-vis absorption spectra of H6TP, EP-PDI and H6TP/EP-PDI solutions in chloroform were shown in Figure 5a. In EP-PDI solution, three strong absorption peaks at 528 nm, 491 nm and 459 nm were observed, which may be attributed to the 0-0, 0-1 and 0-2 transitions of EP-PDI molecules. H6TP solution displayed no apparent absorption in the visible region. After H6TP and EP-PDI were blended, the absorption positions of the solution were the same as that of pure EP-PDI solution. No red-shift or blue-shift of the spectra was observed.

Fluorescence emission spectrum was also performed for further study, as shown in Figure 5b. A wide emission peak at 386 nm was observed in H6TP solution, when excited at 300 nm. For EP-PDI, an emission peak at 582 nm was obtained when the excitation wavelength was 530 nm, and an additional emission peak at 539 nm was also observed when excited at 460 nm. In the blended solutions, when the excitation wavelength was 530 nm, an emission peak corresponding to that of EP-PDI was observed. When excited at 300 nm, the emission spectra represented the superposition of the individual spectra of H6TP and EP-PDI. It was worth to mention that the emission peak at 600 nm was the frequency-doubled peak of the excitation wave. Both UV-vis absorption and fluorescence emission spectroscopy indicated that no

strong donor-acceptor charge transfer interaction was formed in solution.

NMR spectrum has been proved effective to study the interaction between donor and acceptor molecules in solution.<sup>13</sup> We have also obtained <sup>1</sup>H NMR spectra of H6TP, EP-PDI and H6TP/EP-PDI (1/1) in CDCl<sub>3</sub>, which were shown in Figure 5c. The peaks in the NMR spectra could be assigned as follows: H6TP,  $\delta$ =7.83 ppm (s, 6H; ArH), 4.23 ppm (t, 12H; 6OCH<sub>2</sub>), 1.93 ppm (m, 12H; 6CH<sub>2</sub>), 1.20-1.60 ppm (m, 36H; 6(CH<sub>2</sub>)<sub>3</sub>), 0.90 ppm (t, 18H; 6CH<sub>3</sub>); EP-PDI,  $\delta$ =8.67 ppm (d, 4H; ArH), 8.64 ppm (d, 4H; ArH), 5.07 ppm (m, 2H; 2NCH), 2.23-2.28 ppm (m, 4H; 2CH<sub>2</sub>), 1.92-1.98 ppm (m, 4H; 2CH<sub>2</sub>), 0.93 ppm (t, 12H; 4CH<sub>3</sub>). In H6TP/EP-PDI pair, the chemical shift was exactly the superposition of that in H6TP and EP-PDI. No obvious change of the chemical shift was observed. The result further demonstrated that the formation of H6TP/EP-PDI cocrystal was not driven by charge transfer interaction in solution.

### 3.2.2 The Existence of Charge Transfer Interaction in H6TP/EP-PDI Film

DSC was used to characterize the thermal behaviour of H6TP/EP-PDI blend. When H6TP was heated, two endothermic peaks at 67.57°C and 95.20°C were observed, as shown in Figure 6a. These could be assigned to the solid-mesophase and mesophase-isotropic transitions, respectively. Two exothermic peaks at 91.50°C and 52.41°C appeared during the cooling process, which corresponded to the isotropic-liquid crystalline phase and liquid crystalline phase-crystalline phase transitions. As can be seen in Figure 6b, the DSC curve of EP-PDI displayed one phase transition temperature at 73.64°C in the heating procedure and a crystallization

temperature at 66.56°C during the cooling procedure. However, in H6TP/EP-PDI blend with ratio of 1/1, the DSC trace was very different. As shown in Figure 6c, multiple phase transitions peaks at 53.99°C, 62.05°C, 72.74°C and 116.66°C were present upon heating, and exothermic peaks at 112.27°C and 68.35°C were observed upon cooling. The curve exhibited no features ascribable to either of the individual components. Typically, the enhanced phase transition temperature at 116.66°C indicated that strong interaction between H6TP and EP-PDI molecules existed in the bulk, which supplied the donor-acceptor system with additional thermal property. Similar DSC trace was observed when the ratio of H6TP/EP-PDI was 2/1 (see Figure S7). Based on DSC result, it was reasonable to conclude that supramolecular structure was formed in H6TP/EP-PDI blended film.

UV-vis absorption spectra and fluorescence emission spectra of H6TP/EP-PDI films were also performed, the results of which were shown in Figure 7. H6TP film displayed no obvious optical absorption in the visible region. In EP-PDI film, absorption peaks at 592 nm, 550 nm and 502 nm were observed, which could be attributed to the 0-0, 0-1 and 0-2 transitions. The red-shift of the peaks compared to the solution resulted from the crystallization of EP-PDI molecules. In the blended films, we found that the absorption peaks at 592 nm, typical of EP-PDI crystals disappeared. It indicated that the crystallization of individual EP-PDI was inhibited, and H6TP/EP-PDI cocrystal formed. Fluorescence emission spectra provided further evidence. As can be seen in Figure 7b, a wide emission peak at 420 nm was observed in H6TP film, when excited at 300 nm. The emission peak at 600 nm was the

frequency-doubled peak of the excitation wave at 300 nm, as aforementioned. For EP-PDI, an emission peak at 625 nm was obtained when excited at 470 nm. However, in the blended films, fluorescence quenching was observed, especially in the region of emission peak of EP-PDI. The phenomenon was accordant to the fluorescence microscopy images shown in Figure S3 and indicated that strong charge transfer interaction existed in the film, resulting from the formation of H6TP/EP-PDI cocrystal.

### **3.2.3 Driving Force for the Assembly of H6TP/EP-PDI Cocrystal: $\pi$ - $\pi$ Interaction and Steric Hindrance Effect**

Hydrogen bond, charge transfer (CT) state and  $\pi$ - $\pi$  interaction were reported to be the driving force of organic cocrystal. Based on the chemical structures of H6TP and EP-PDI (Scheme 1), hydrogen bond was firstly excluded in the system, because no -OH, -NH<sub>2</sub> or -COOH existed. Besides, we did not observe charge transfer state in H6TP/EP-PDI solution.  $\pi$ - $\pi$  interaction between H6TP and EP-PDI molecules seemed to be the main driving force for the formation of the cocrystal. It was reasonable because the diffractive peak of  $\pi$ - $\pi$  stacking was observed only in the blended film, according to the in-plane XRD profiles. Fluorescence emission spectra also indicated that alternating stacking of H6TP/EP-PDI may form. We thus ensured that in H6TP/EP-PDI cocrystal, the donor and acceptor molecules stacked alternately through  $\pi$ - $\pi$  interaction. The electrical complementation may supply additional Coulomb force, which favored the co-assembly between the molecules.

The smaller side groups of the molecules may be another factor for the assembly of

the cocrystal, because the weaker steric hindrance favored the stacking of H6TP/EP-PDI central cores. To support our opinion, 2,3,6,7,10,11-hexakis-(hexylthio)-triphenylene (HHTT), possessing the same core to H6TP but larger side groups, was blended with EP-PDI. As shown in Figure S8, we did not observe obvious shift of the diffractive peak in the blended film, based on GIXD profile. Much weaker diffractive peak of  $\pi$ - $\pi$  stacking was observed in the in-plane XRD profile. We argued that the larger steric hindrance inhibited the stacking between HHTT and EP-PDI molecules, and crystals of individual components dominated in the film.

### 3.3 Electrical Performance of H6TP/EP-PDI Cocrystal

In order to characterize the electrical performance of H6TP/EP-PDI cocrystal, FETs with bottom gate, top contact configuration were fabricated. As shown in Figure 8, V-shaped transfer curves with one arm indicating electron (n-type) transport and the other indicating hole (p-type) transport were observed. The ambipolar transport characteristic was attributed to the superexchange nature along the  $\pi$ -stacking direction in the cocrystal<sup>4</sup>. The mobility was calculated using the formula below.

$$\mu = \frac{2L}{WC_i} \left( \frac{\partial \sqrt{I_{SD}}}{\partial V_G} \right)^2 \quad (1)$$

Relatively balanced hole/electron transport was obtained. In the drop-cast film, the electron and hole mobilities were  $1.40 \times 10^{-3} \text{ cm}^2/\text{Vs}$  and  $1.14 \times 10^{-3} \text{ cm}^2/\text{Vs}$ , respectively ( $\mu_e/\mu_h=1.23$ ). In the spin-coated film, the electron and hole mobilities were  $3.74 \times 10^{-4} \text{ cm}^2/\text{Vs}$  and  $2.40 \times 10^{-4} \text{ cm}^2/\text{Vs}$  ( $\mu_e/\mu_h=1.56$ ). The lower mobilities in the spin-coated film were due to the smaller sizes of H6TP/EP-PDI cocrystals.

Although the obtained hole/electron mobility was low, we argued that organic donor-acceptor cocrystal with alternating stacking structure could be further applied in organic electronics.

#### 4. CONCLUSIONS

In summary, we have prepared organic donor-acceptor cocrystal based on H6TP and EP-PDI molecules. Both the morphology and the crystalline structure of the cocrystal were different from that of the individual crystal. In the cocrystal, an alternating stacking of H6TP and EP-PDI molecules was predicted. The formation of the cocrystal was attributed to the  $\pi$ - $\pi$  interaction between the donor and the acceptor. The weaker steric hindrance may also favor the assembly between H6TP and EP-PDI molecules. Ambipolar transport property was observed in H6TP/EP-PDI cocrystal, with hole mobility of  $1.14 \times 10^{-3} \text{ cm}^2 \text{ V}^{-1} \text{ s}^{-1}$  and electron mobility of  $1.40 \times 10^{-3} \text{ cm}^2 \text{ V}^{-1} \text{ s}^{-1}$ .

#### Acknowledgment

This work was supported by the National Natural Science Foundation of China (51273191, 21474113), the National Basic Research Program of China (973 Program-2014CB643505), the Strategic Priority Research Program of the Chinese Academy of Sciences (Grant No. XDB12020300).

## References

- (1) L. S. Mende, A. Fechtenkötter K.Müllen, E. Moons, R. H. Friend and J. D. MacKenzie, *Science*, 2001, **293**, 1119-1122.
- (2) S. J. Kang, S. Ahn, J. B. Kim, C. Schenck, A. M. Hiszpanski, S. Oh, T. Schiros, Y. L. Loo and C. Nuckolls, *J. Am. Chem. Soc.*, 2013, **135**, 2207-2212.
- (3) M. Kumar, K. V. Rao and S. J. George, *Phys. Chem. Chem. Phys.*, 2014, **16**, 1300-1313.
- (4) L. Y. Zhu, Y. P. Yi, Y. Li, E. G. Kim, V. Coropceanu J. L. Brédas, *J. Am. Chem. Soc.*, 2012, **134**, 2340-2347.
- (5) S. K. Park, S. Varghese, J. H. Kim, S. Yoon, O. K. Kwon, B. An, J. Gierschner and S. Y. Park, *J. Am. Chem. Soc.*, 2013, **135**, 4757-4764.
- (6) J. Zhang, J. H. Tan, Z. Y. Ma, W. Xu, G. Y. Zhao, H. Geng, C. Di, W. P. Hu, Z. G. Shuai, K. Singh and D. B. Zhu, *J. Am. Chem. Soc.*, 2013, **135**, 558-561.
- (7) A. S. Tayi, A. K. Shveyd, A. C. H. Sue, J. M. Szarko, B. S. Rolczynski, D. Cao, T. J. Kennedy, A. Sarjeant, C. L. Stern, W. F. Paxton, W. Wu, S. K. Dey, A. C. Fahrenbach, J. R. Guest, H. Mohseni, L. X. Chen, K. L. Wang, J. F. Stoddart and S. I. Stupp, *Nature*, 2012, **488**, 485-489.
- (8) P. Jonkheijm, N. Stutzmann, Z. J. Chen, D. M. de Leeuw, E. W. Meijer, A. P. H. J. Schenning and F. Würthner, *J. Am. Chem. Soc.*, 2006, **128**, 9535-9540.
- (9) F. Würthner, Z. J. Chen, F. J. M. Hoeben, P. Osswald, C. C. You, P. Jonkheijm, J. v. Herrikhuyzen, A. P. H. J. Schenning, P. P. A. M. vander Schoot, E. W. Meijer, E. H. A. Beckers, S. C. J. Meskers and R. A. J. Janssen, *J. Am. Chem. Soc.*, 2004,

- 126**, 10611-10618.
- (10) K. Ariga, J. P. Hill, M. V. Lee, A. Vinu, R. Charvet and S. Acharya, *Sci. Technol. Adv. Mater.*, 2008, **9**, 014109.
- (11) D. Venkataraman, S. Yurt, B. H. Venkatraman and N. Gavvalapalli, *J. Phys. Chem. Lett.*, 2010, **1**, 947-958.
- (12) F. J. M. Hoeben, P. Jonkheijm, E. W. Meijer and A. P. H. J. Schenning, *Chem. Rev.*, 2005, **105**, 1491-1546.
- (13) L. M. Klivansky, D. Hanifi, G. Koshkakaryan, D. R. Holycross, E. K. Gorski, Q. Wu, M. H. Chai and Y. Liu, *Chem. Sci.*, 2012, **3**, 2009-2014.
- (14) G. De Luca, A. Liscio, M. Melucci, T. Schnitzler, W. Pisula, C. G. Clark, Jr, L. M. Scolaro, V. Palermo, K. Müllen and P. Samori, *J. Mater. Chem.*, 2010, **20**, 71-82.
- (15) H. Imahori and F. Fukuzumi, *Adv. Funct. Mater.*, 2004, **14**, 525-536.
- (16) P. W. Boyd and C. A. Reed, *Acc. Chem. Res.*, 2005, **38**, 235-242.
- (17) J. Y. Wang, J. Yan, L. Ding, Y. G. Ma and J. Pei, *Adv. Funct. Mater.*, 2009, **19**, 1746-1752.
- (18) L. Y. Park, D. G. Hamilton, E. A. McGehee and K. A. McMenimen, *J. Am. Chem. Soc.*, 2003, **125**, 10586-10590.
- (19) E. O. Arikainen, N. Boden, R. J. Bushby, O. R. Lozman, J. G. Vinter and A. Wood, *Angew. Chem. Int. Ed.*, 2000, **39**, 2333-2336.
- (20) J. J. Reczek, K. R. Villazor, V. Lynch, T. M. Swager and B. L. Iverson, *J. Am. Chem. Soc.*, 2006, **128**, 7995-8002.
- (21) T. Kreouzis, K. Scott, K. J. Donovan, N. Boden, R. J. Bushby, O. R. Lozman, Q.

- Liu, *Chem. Phys.*, 2000, **262**, 489-497.
- (22) A. Pecchia, O. R. Lozman, B. Movaghar, N. Boden and R. J. Bushby, *Phys. Rev. B*, 2002, **65**, 104204.
- (23) B. R. Wegewijs and L. D. A. Siebbeles, *Phys. Rev. B*, 2002, **65**, 245112.
- (24) P. S. Kumar, S. Kumar and V. Lakshminarayanan, Electrical Conductivity Studies on Discotic Liquid Crystal-Ferrocenium Donor-Acceptor Systems. *J. Phys. Chem. B*, 2008, **112**, 4865-4869.
- (25) N. Boden, R. J. Bushby, Z. B. Lu and O. R. Lozman, *Liq. Cryst.*, 2001, **28**, 657-661.
- (26) W. Pisula, M. Kastler, D. Wasserfallen, J. W. Robertson, F. Nolde, C. Kohl and K. Müllen, *Angew. Chem. Int. Ed.*, 2006, **45**, 819-823.
- (27) G. Cooke, V. Sage and T. Richomme, *Synth. Commun.*, 1999, **29**, 1767-1771.
- (28) V. Percec, E. Aqad, M. Peterca, M. R. Imam, M. Glodde, T. K. Bera, Y. Miura, V. S. K. Balagurusamy, P. C. Ewbank, F. Würthner and P. A. Heiney, *Chem. Eur. J.*, 2007, **13**, 3330-3345.
- (29) K. Balakrishnan, A. Datar, R. Oitker, H. Chen, J. M. Zuo and L. Zang, *J. Am. Chem. Soc.*, 2005, **127**, 10496-10497.
- (30) M. Wiatrowski, E. Dobruchowska, W. Maniukiewicz, U. Pietsch, J. Kowalski, J. Ulanski and Z. Szamel, *Thin Solid Films*, 2010, **518**, 2266-2270.
- (31) G. Koshkakarayan, P. Jiang, V. Altoe, D. Cao, L. M. Klivansky, Y. Zhang, S. Chung, A. Katan, F. Martin, M. Salmeron, B. Ma, S. Aloni and Y. Liu, *Chem. Commun.*, 2010, **46**, 8579-8581.

**TABLE CAPTION**

**Table 1.** A summary of the physical parameters of chlorobenzene and chloroform.

**FIGURE CAPTIONS**

**Scheme 1.** The chemical structures of H6TP and EP-PDI molecules.

**Figure 1.** POM images of drop-cast H6TP/EP-PDI films with different ratios by weight. The ratios of H6TP/EP-PDI were (a) 1/0, (b) 4/1, (c) 3/1, (d) 2/1, (e) 1/1, (f) 1/2, (g) 1/3, (h) 1/4 and (i) 0/1, respectively. The solvent used was chloroform and the total solute concentration was 5 mg/ml.

**Figure 2.** (a) AFM images of spin-coated H6TP/EP-PDI films. The solvent used was chloroform and the concentration was 5 mg/ml. The ratios of H6TP/EP-PDI were (a1) 1/0, (a2) 2/1, (a3) 1/1 and (a4) 0/1, respectively. The corresponding TEM and SAED images were shown below. (b) GIXD profiles of the corresponding films.

**Figure 3.** (a) GIXD and (b) in-plane XRD profiles of drop-cast H6TP/EP-PDI films with different ratios by weight. (a2) and (b2) highlight the diffractive profiles at optimized ratio of H6TP/EP-PDI. The solvent used was chloroform and the concentration was 5 mg/ml.

**Figure 4.** Schematic representation of the crystalline structures of (a) EP-PDI, (b) H6TP and (c) H6TP/EP-PDI cocrystal.

**Figure 5.** (a) UV-vis absorption spectra and (b) fluorescence emission spectra of H6TP, EP-PDI and H6TP/EP-PDI chloroform solutions. The wavelength (300 nm, 460 nm, 530 nm) in the inset of (b) indicated the excitation wavelength. (c)  $^1\text{H}$  NMR spectra of H6TP, EP-PDI and H6TP/EP-PDI (1/1) in  $\text{CDCl}_3$ .

**Figure 6.** DSC curves of (a) H6TP, (b) EP-PDI and (c) H6TP/EP-PDI (1/1).

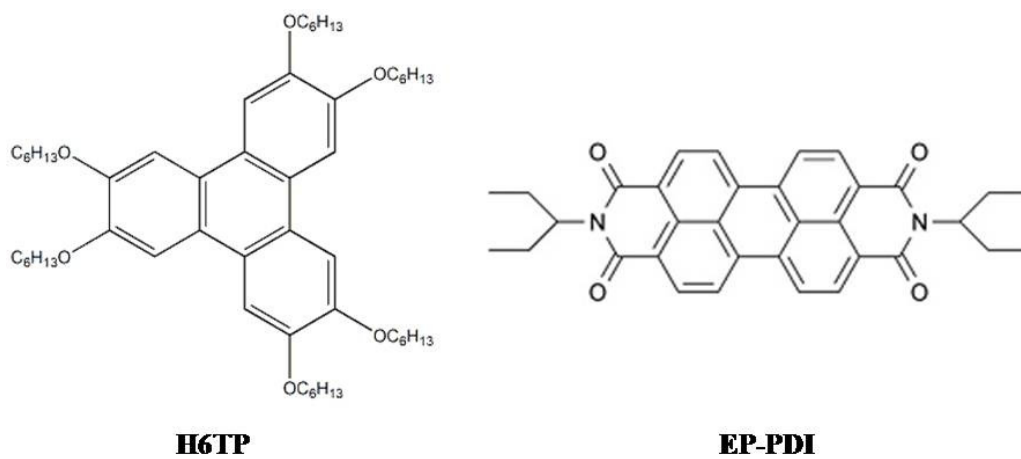
**Figure 7.** (a) UV-vis absorption spectra and (b) fluorescence emission spectra of H6TP, EP-PDI and H6TP/EP-PDI (2/1, 1/1) films. The films were prepared through drop-casting from corresponding chloroform solutions.

**Figure 8.** Typical characteristic transfer curves of OFETs based on (a) drop-cast and (b) spin-coated H6TP/EP-PDI (1/1) films. The insert indicated the corresponding POM image of the film between the source and drain electrodes. The channel length (L) and width (W) were 200  $\mu\text{m}$  and 6 mm, respectively.

**Table 1.**

<b>Solvent</b>	<b>Boiling point (°C)</b>	<b>Viscosity (mPa·s)</b>	<b>solubility parameter (cal/cm<sup>3</sup>)<sup>1/2</sup></b>
Chlorobenzene	131.7	0.730	9.54
Chloroform	61.3	0.539	9.30

Scheme 1.



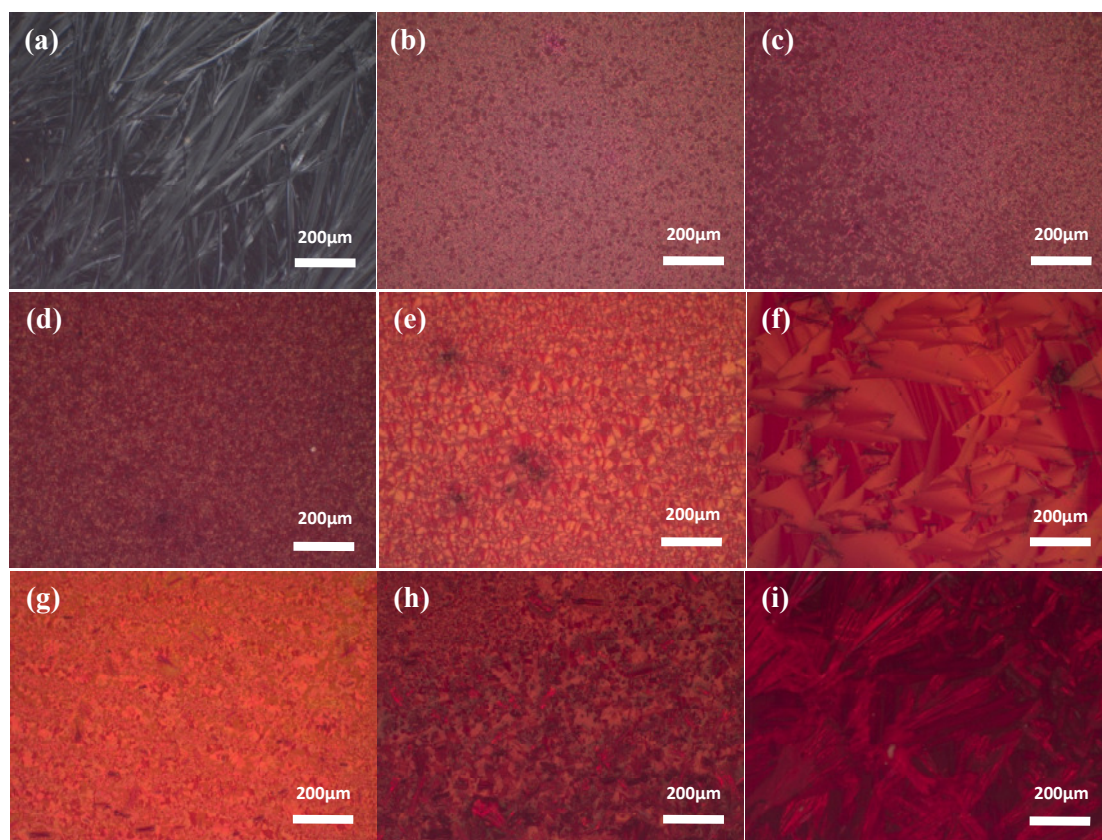
**Figure 1.**

Figure 2.

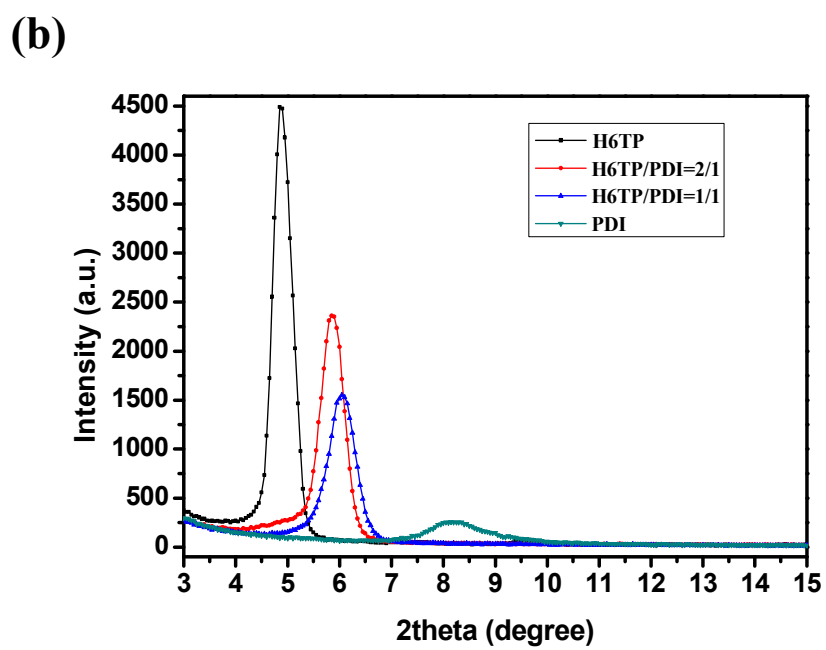
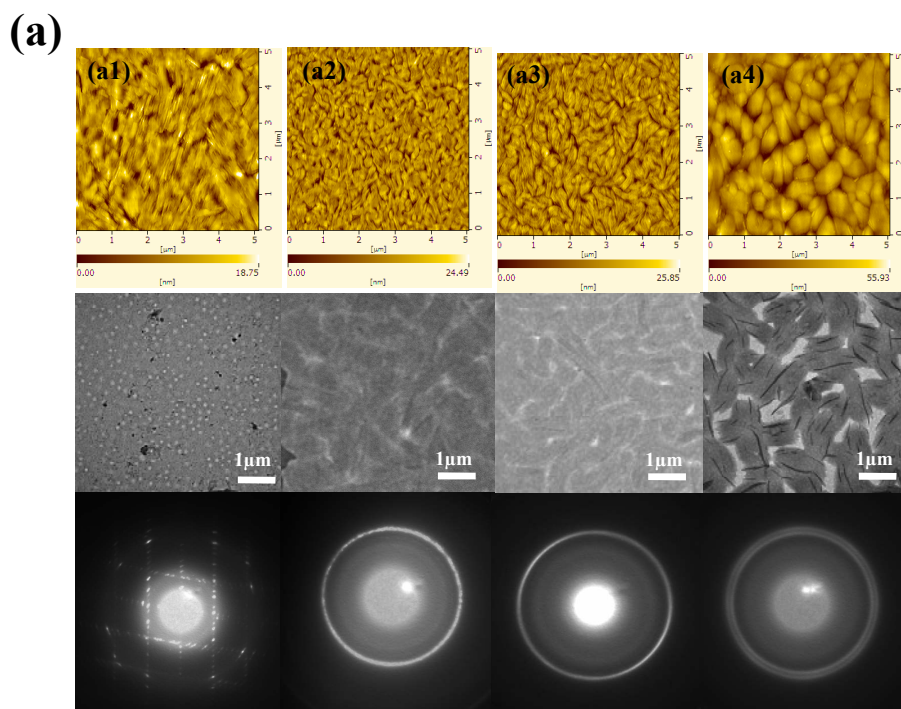
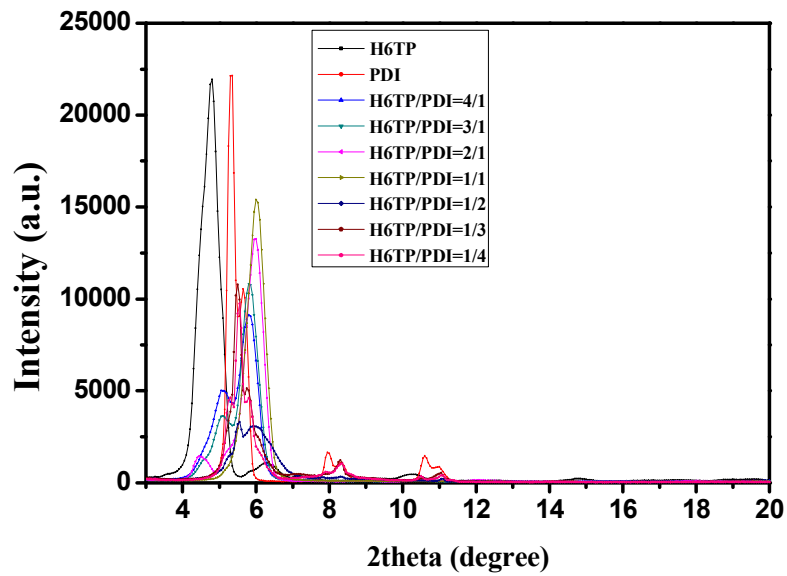
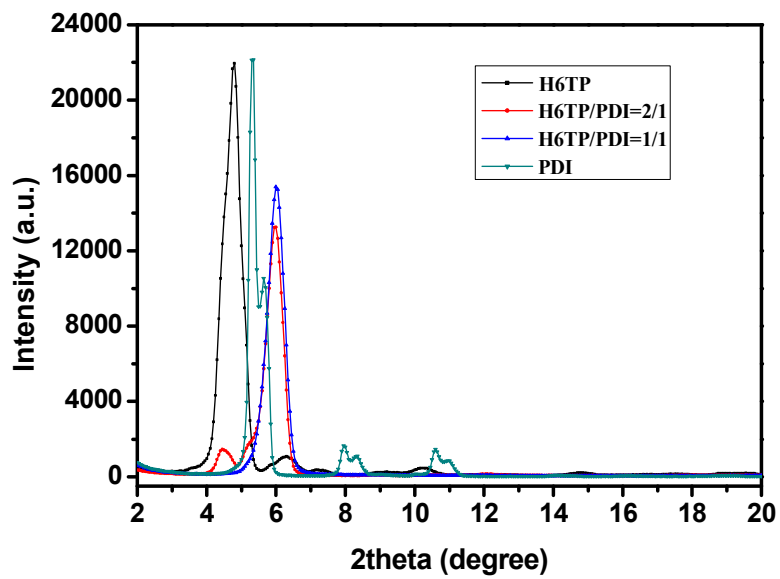


Figure 3.

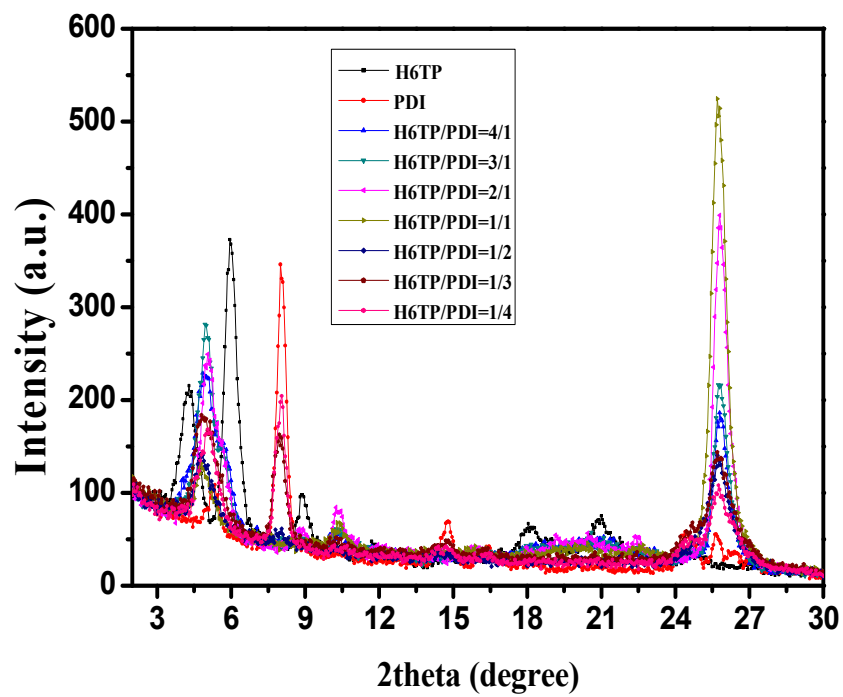
(a1)



(a2)



(b1)



(b2)

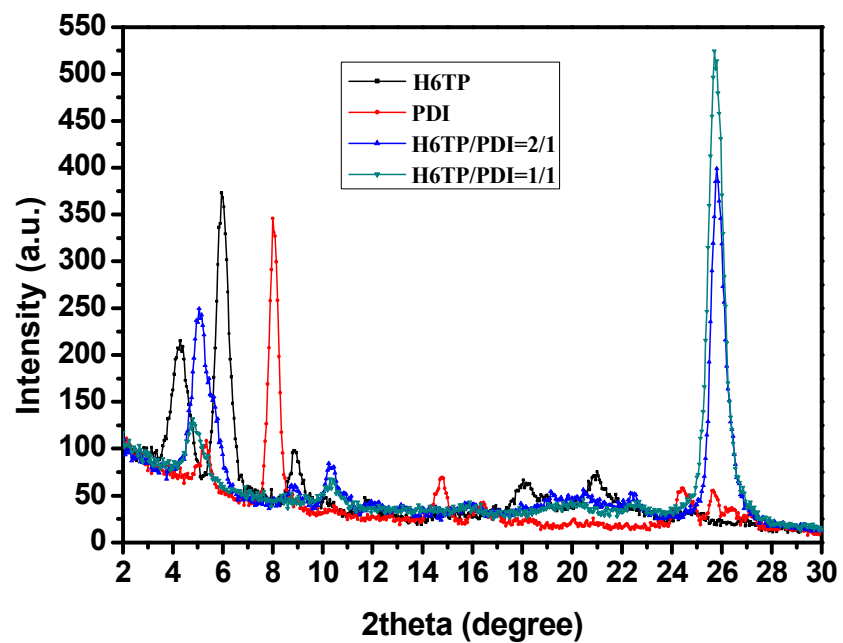


Figure 4.

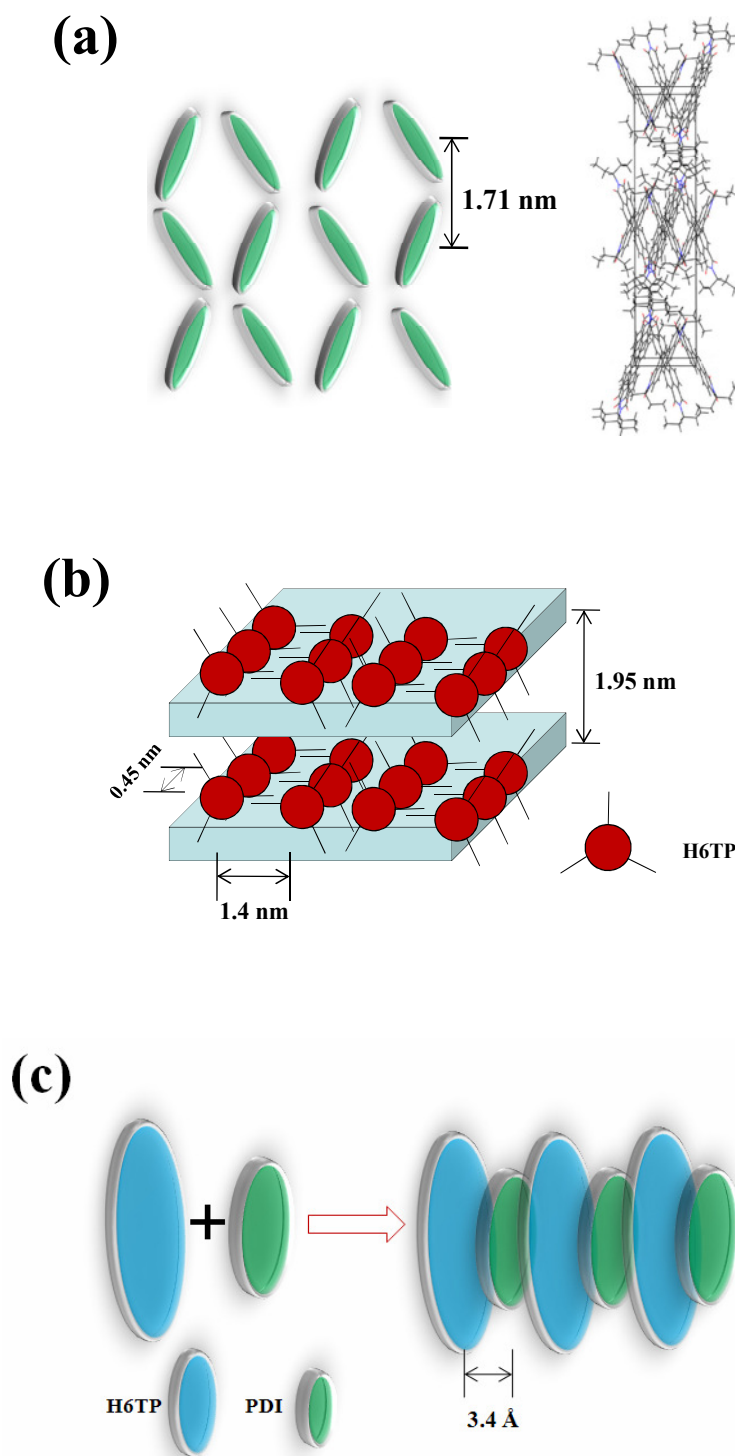
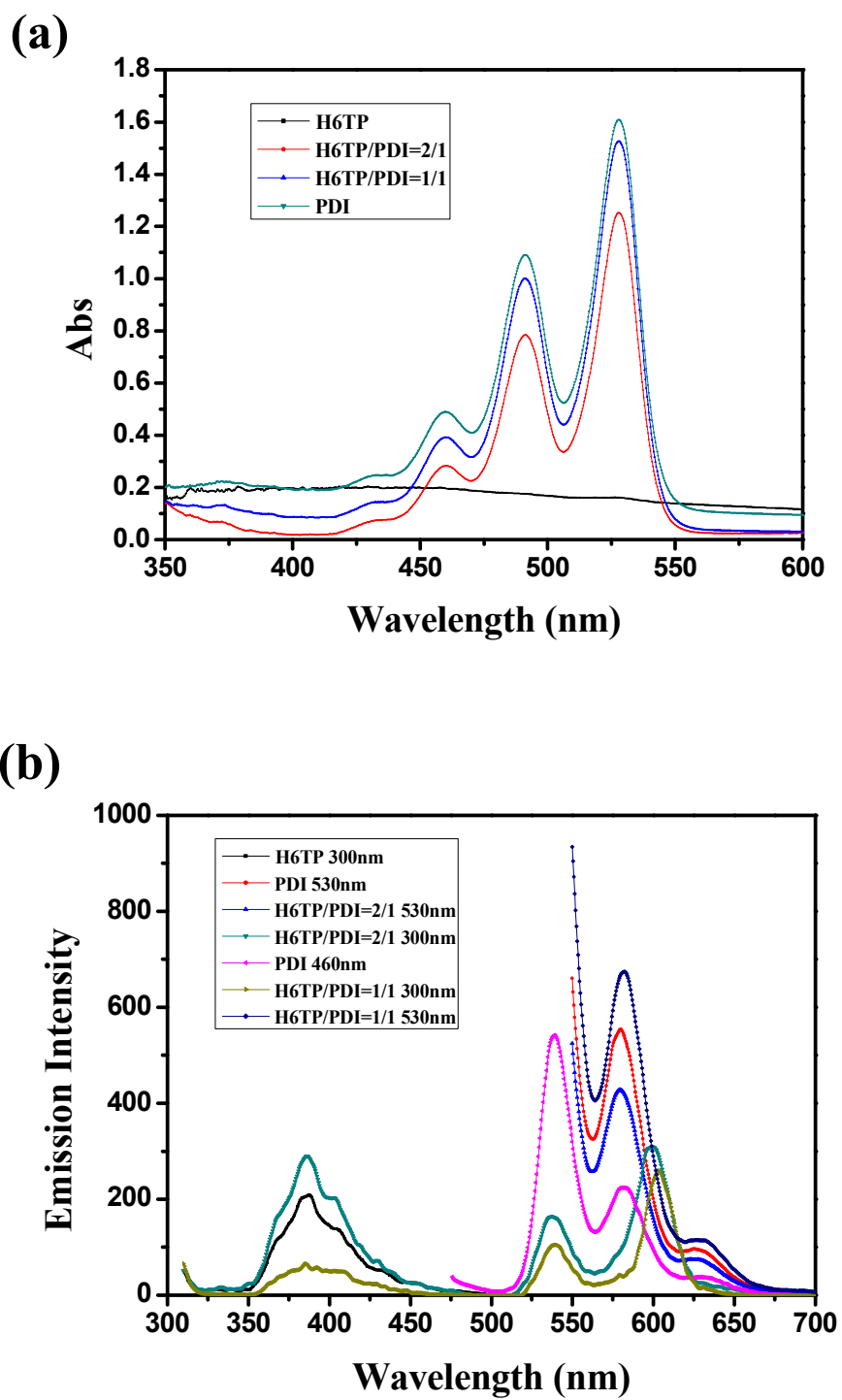


Figure 5.



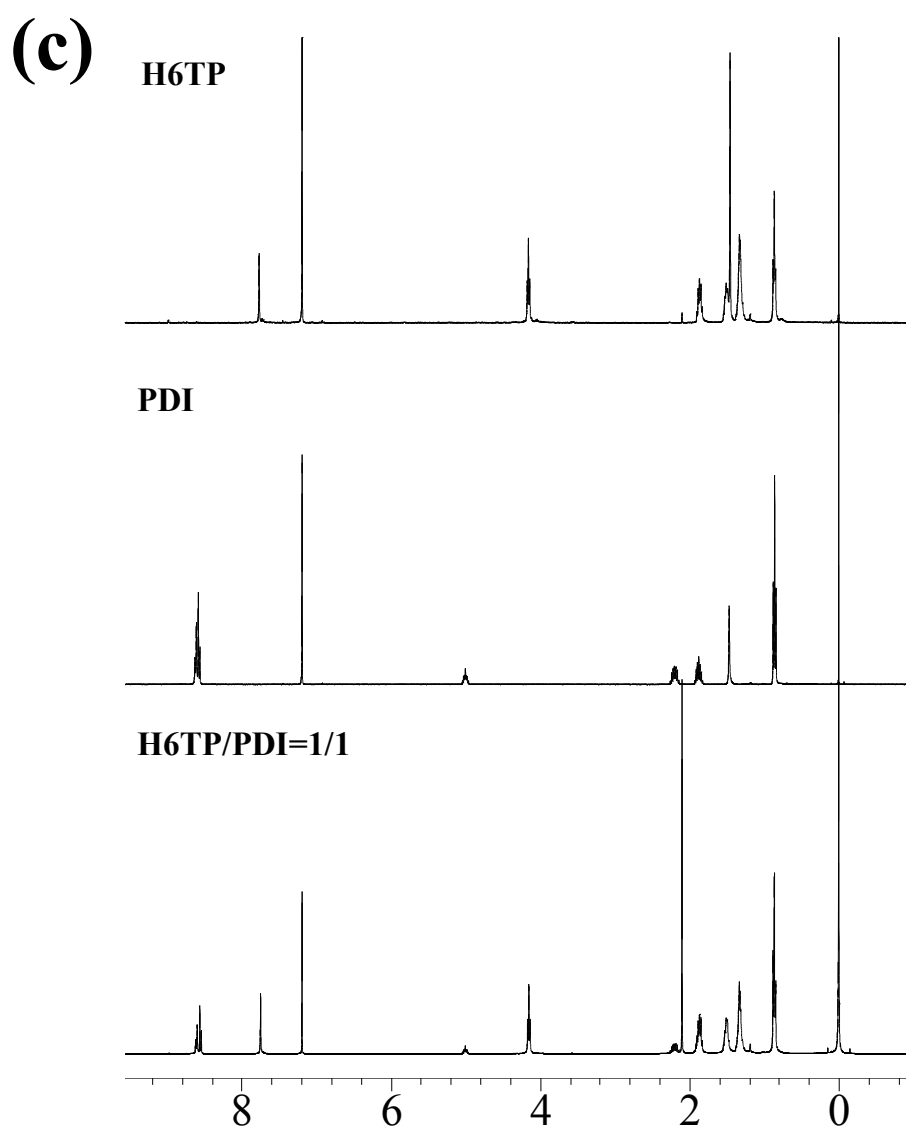
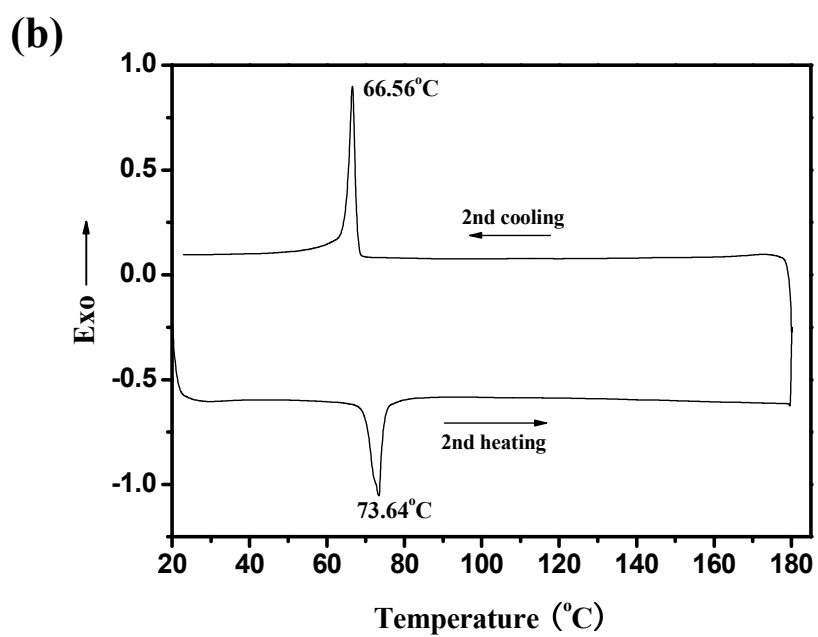
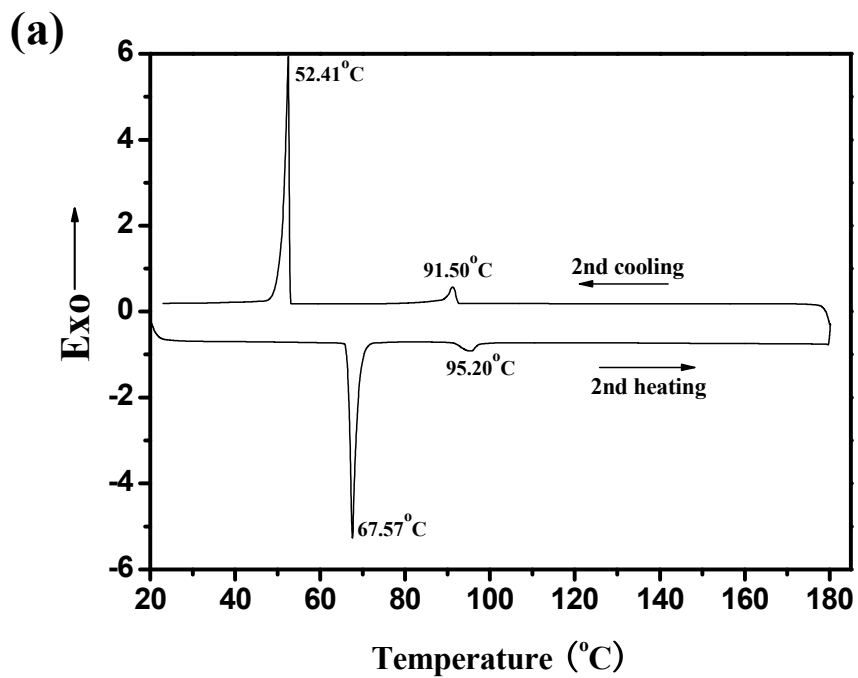


Figure 6.



(c)

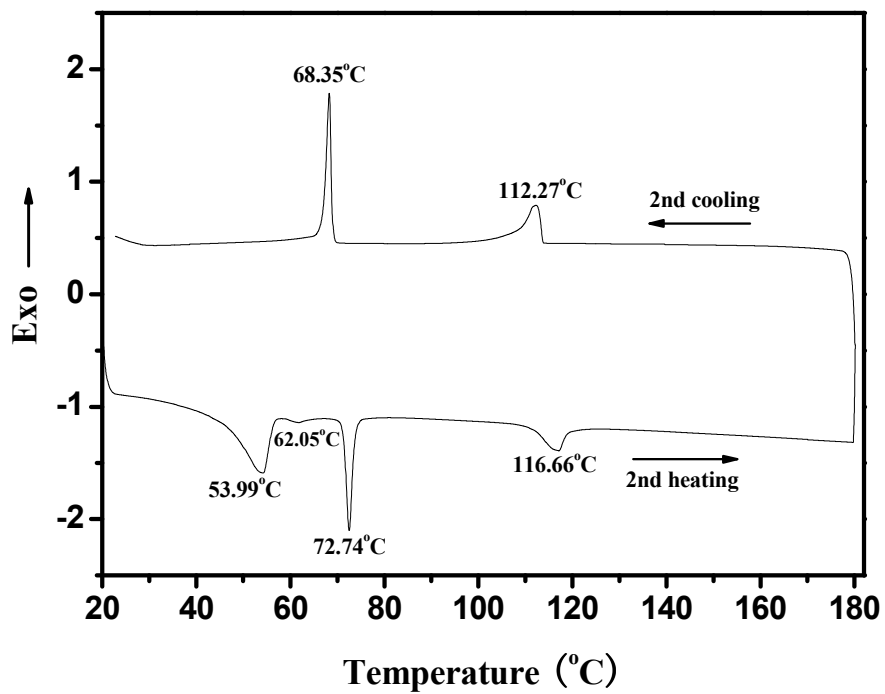


Figure 7.

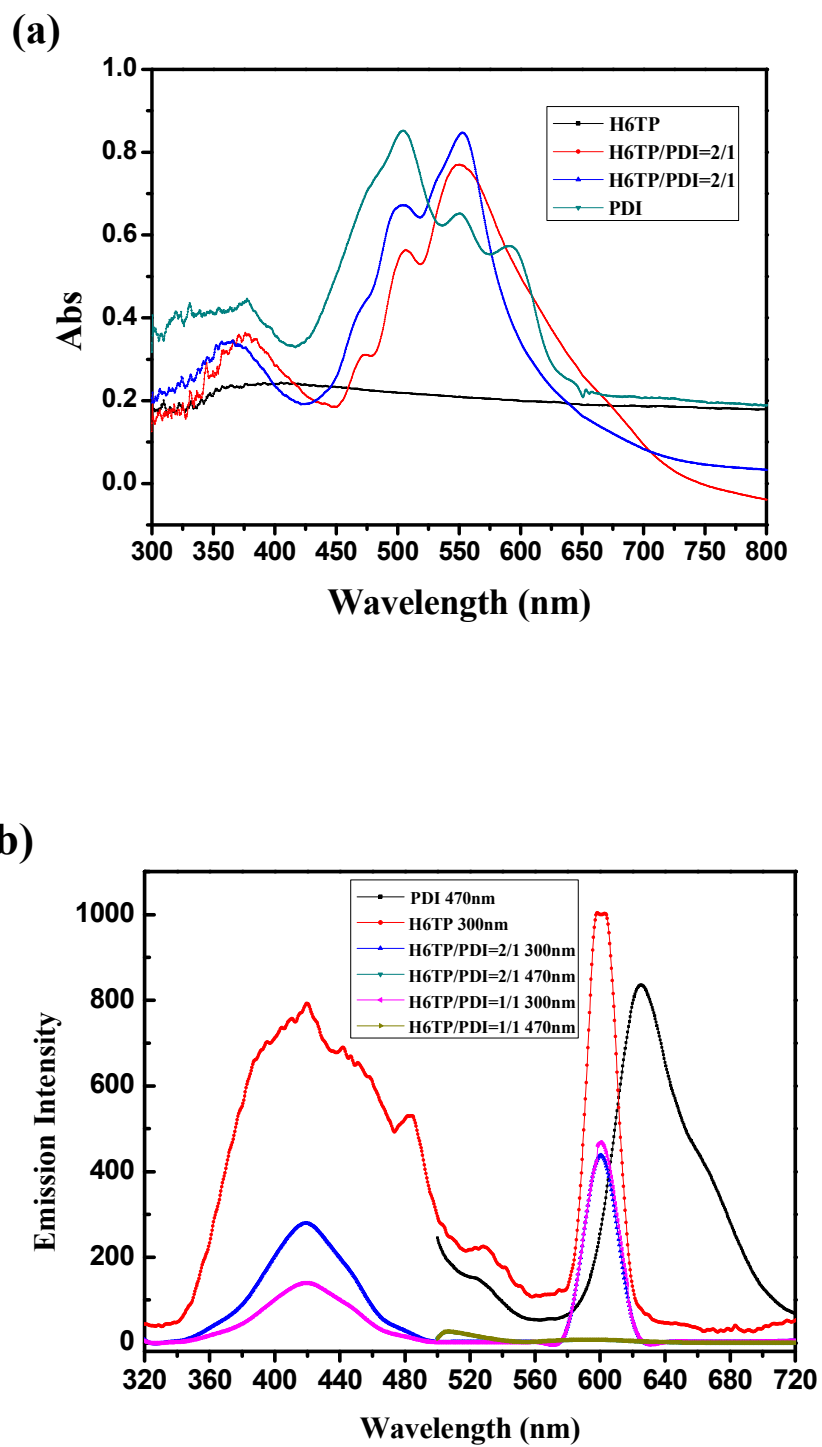


Figure 8.

